A MULTI-SCALE MODELLING METHOD FOR TUFTED COMPOSITES: UNIT-CELL MODEL

C. Osmiani[1], G. Mohamed[1], G. Allegri[2] and I. K. Partridge[1]

[1]Advanced Composites Centre for Innovation and Science, Department of Aerospace Engineering, University of Bristol, Bristol BS8 1TR, United Kingdom
Email: camilla.osmiani@bristol.ac.uk, Web Page: http://www.bristol.ac.uk/composites/
[2]Faculty of Engineering, Department of Aeronautics, Imperial College London, London SW7 2AZ, United Kingdom
Email: g.allegri@imperial.ac.uk, Web Page: https://www.imperial.ac.uk/

Keywords: Through-thickness reinforcement, Multi-scale modelling, FE analysis

Abstract
The number of applications of through-the-thickness reinforcement at industrial level is currently limited, especially in relation to the relatively recent tufting technique. One identified reason for this is the absence of efficient modelling tools capable of accounting for tufts in the design process and of accurately predicting their potential benefits and/or negative effects on the final performance of a component [1]. The aim of this research is to provide a deeper understanding of the energy dissipation mechanisms exerted by tufts under various loading conditions and their inclusion in finite element models capable of predicting the response to delamination of tufted composite structures. With focus on the 'micro-local' scale of the problem, the characterization of the mode I bridging law of single carbon tufts is reported in this paper, and a strategy for model development is proposed.

1. Introduction

Tufting represents the simplest approach to one-sided stitching and it considerably improves the damage tolerance of dry-preform based 2D composites, while facilitating the assembly of structural and non-structural parts. To date, the design of tufted structures has relied primarily on empirical data. This is due to the absence of robust modelling tools capable of predicting the toughening action of tufted Through-Thickness Reinforcement (TTR) and the associated benefits and/or negative effects (e.g. in-plane strength reduction) on the final performance of a structural component [1]. Existing literature identifies multi-scale modelling as the most appropriate strategy for dealing with through-the-thickness reinforced composites [2, 3]. Three main length scales, or levels, are usually considered: the smaller is concerned with the 'bridging law' of the individual micro-fasteners (e.g. tufts and Z-pins) and is referred to as 'level-1 meso-scale'. Non-linear springs and cohesive elements (or combinations of the two) are then adopted to represent the bridging action of TTRs into larger scale Finite Element (FE) models ('level-2 meso-scale' and 'macro-scale') [4], respectively aimed at predicting the response of bridged interfaces and the overall failure modes of through-thickness reinforced composite parts.

This paper focuses on 'micro-local' scale (or level-1 meso-scale) modelling. In particular, a strategy for the development of a unit cell finite element model for tufted composites is proposed. This model is not only meant to deepen our understanding of the energy dissipation mechanisms associated with tufting during delamination bridging, but, once finalised, will become a tool for the prediction of the bridging laws of tufts having arbitrary architectures in a general mixed-mode regime.

Excerpt from ISBN 978-3-00-053387-7

2. Tuft bridging mechanisms: mode I

2.1. Experimental characterisation

The finite element model presented in this paper has been informed by the morphology and mechanical behaviour of a set of pre-delaminated single-tuft coupons tested in pull-out (mode I). These 20 x 20 mm coupons were cut out of a carbon biaxial Non Crimp Fabric (NCF) - epoxy panel with $[0/90, (90/0)_7]_s$ layup. The fabric plies in the dry preform were separated by a 20 μm thin layer of release film, placed at the symmetry plane of the stack, and were tufted with 2k HTA40 carbon fibre thread. The tufted preform was infused with a low-curing-temperature epoxy (Momentive RIMR 935/RIMH 936), using a Vacuum Assisted Resin Transfer Moulding (VARTM) process. The infusion was run at 35°C. The impregnated preform was cured at 60°C for 2 hours and post-cured at 80°C for 1.5 hours. The single-tuft coupons have an average thickness of 6.56 mm (Coefficient Of Variation (COV) = 1.42 %), resulting in a global fibre volume fraction of 60.5 %. Mechanical load was applied to the specimens using a 1 kN load cell in displacement-controlled mode, at a cross-head speed of 0.5 mm/min. The relative opening displacement of the two halves of each specimen was recorded using an Imetrum Video Gauge® apparatus. The experimental setup is shown in Fig. 1.

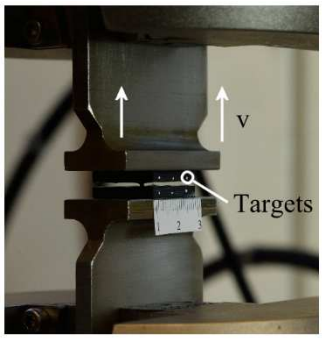

Figure 1. Experimental setup for the single-tuft pull-out test. The position and relative displacement of the targets have been monitored using a video gauge system.

2.2. Tuft morphology

Micrographic analysis and X-ray tomography have been selected for the in-plane and out-of-plane characterisation of the topological features of the tufts. It is important to remark that, in the context of this paper, a 'tuft' consists of two resin-impregnated segments of sewing thread; the tuft is co-cured with the preform it is inserted in, becoming part of the "locally 3D" fibre architecture of the composite. Unlike Z-pins, tufts do not have a constant cross-sectional arrangement, but their cross-section is shaped by the in-plane fibre architecture and layup of the preform. When the threaded tufting needle penetrates the preform, the in-plane fibres of the fabric are first moved apart; upon needle retraction, they wrap around the tuft. The entity of this "closure" varies depending on the stacking sequence of the fabric and it is maximum in unidirectional composites, where tufts display a cross-section elongated in the in-plane fibre direction. This local fibre misalignment causes the formation of resin rich regions around the tufts, as shown in Fig. 2a, which is a common characteristic of through-thickness reinforced composites [5].

In the thickness direction, the morphology of tufts is mainly influenced by the fibre architecture of the reinforcing thread (Fig. 2b). This architecture is defined by the number of yarns and by the twisting level of the thread. In the tested coupons, for example, the tufting thread was made of two interlaced yarns, each following a helical path with a 5.1 mm pitch. The direct consequence of this feature is that

Excerpt from ISBN 978-3-00-053387-7

tufts are mechanically interlocked with the surrounding medium, unlike z-pins which are simply in frictional contact with the embedding laminate.

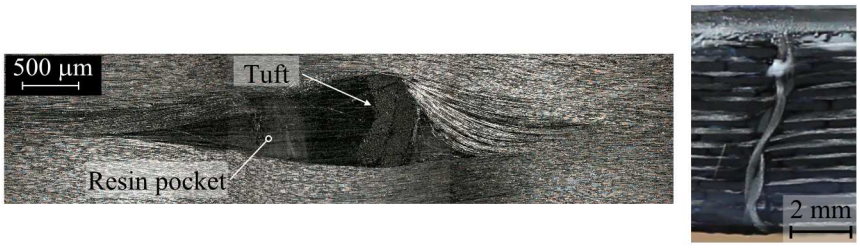

Figure 2. Micrograph showing the in-plane morphology of a tufted 0°/90° NCF composite, at the tuft location (left) and its through-thickness section (right). The tufting thread is made of 2k HTA40 carbon fibres.

2.3. Single-tuft bridging law

A representative mechanical response of a pre-delaminated single-tuft coupon tested in mode I is presented in Fig. 4c. X-ray analysis of the pristine specimen (Fig. 4a) shows that the tuft was initially fully bonded to the composite. In the first stage of its mode I response, the bonded tuft exhibits a quasi-linear behaviour. Displacements are in the order of 0.02 mm and materials can be considered to behave elastically. Upon reaching a characteristic load threshold, which for the tested specimens has been estimated in the range 100-150 N, the compliance of the tuft increases significantly. Fig. 4b shows evidence of interfacial de-bonding along the tuft. This is considered to be responsible for the observed stiffness reduction, whereas sudden load drops could be connected to internal fibre-matrix splitting [6]. When the applied displacement approaches its ultimate value, progressive brittle tensile fibre failure occurs in the tuft strands separated by the splits, and the broken tuft exhibits a broom like fracture, as in Fig. 5.

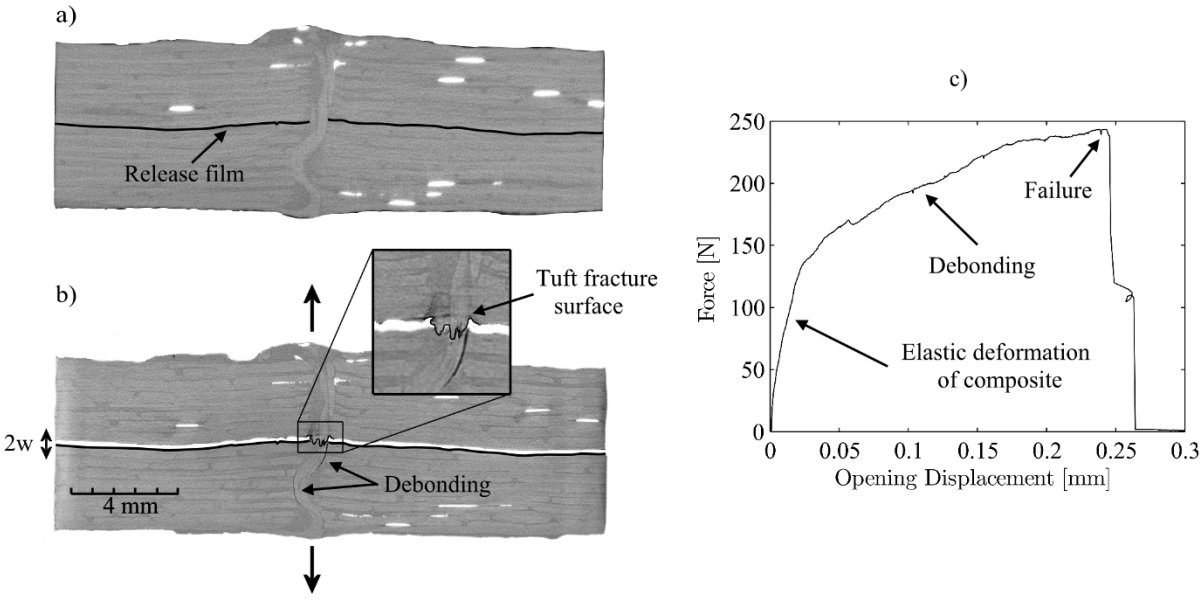

Figure 4. X-ray image of a pristine (a) and failed (b) single-tuft specimen. The bridging law of the tuft in object and its failure mechanisms are is reported in (c).

Excerpt from ISBN 978-3-00-053387-7

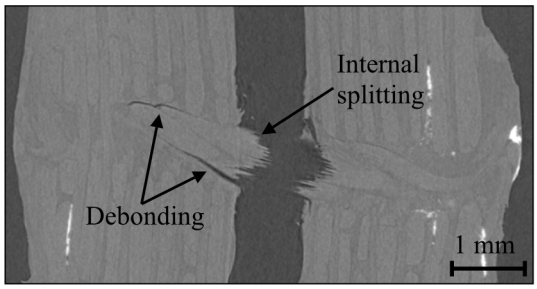

Figure 5. Close-up of a failed tuft (X-ray image) showing interfacial debonding and splitting of the fibres in the yarns.

3. Modelling strategy

A level-1 meso-scale finite element model for tufted composites, as presented in this paper, is an instrument for the identification of the energy dissipation mechanisms affecting tufts when bridging across interlaminar cracks. This process of identification is a pre-requisite for building design tools capable of *a priori* predicting the response of tufted composites. This section discusses the main issues involved in the process of model development and identifies the parameters which most influence the performance of the model. Albeit currently limited to mode I scenarios, these considerations will be in the future extended to mixed-mode regimes.

3.1. Geometry definition and material properties

Considered the substantial differences in the *in-situ* morphology of tufts, even within the same preform, the geometry of the tuft in the model needs to be idealised, while still being representative of the system it is due to describe. Here the tuft is described as formed by two adjacent thread segments. The yarns in each thread segment are modelled, using a continuum approach, as helical cylinders with circular cross section. The helical pitch of the cylinders is defined by the fibre architecture of the tufting thread, whereas their cross sectional area is derived from the observed *in-situ* cross-sectional area of the tufts (see Fig. 2). The yarns are assumed to be transversely isotropic and to have elastic behaviour to failure. 3D homogenised material properties are assigned to them, determined by accounting for the average *in-situ* volume fractions of fibres and resin in the tufts (Chamis' material model for unidirectional composites [7] has been used to derive the values of the elastic constants reported in Table 1). The material orientation for the yarns is defined so that the 1-material axis follows the helical path of each yarn.

Table 1. Elastic constants for FE simulation

	E_1 (GPa)	E_2 (GPa)	E_3 (GPa)	ν_{12} (-)	ν_{13} (-)	ν_{23} (-)	G_{12} (GPa)	G_{13} (GPa)	G_{23} (GPa)
Yarn	146.0	8.0	8.0	0.259	0.259	0.405	4.01	4.01	2.71
Resin	2.8	2.8	2.8	0.4	0.4	0.4			
Composite	81.8	81.8	8.4	0.028	0.141	0.141	3.56	2.90	2.90

Excerpt from ISBN 978-3-00-053387-7

Table 2. Coefficients of Thermal Expansion (CTE) for thermal analysis

	α_1 (K^{-1})	α_2 (K^{-1})	α_3 (K^{-1})
Yarn	1.27E-7	1.17E-5	1.17E-5
Resin	3E-5	3E-5	3E-5
Composite	1.29E-6	1.29E-6	4.17E-5

The resin rich region around the tuft is modelled as an isotropic hollow cylinder with dimensions dictated by the average local tuft/resin volume fractions of the composite (tuft area/ resin pocket area). For common quasi-isotropic and 0°/90° composite panels, the actual shape of the resin pockets has no influence on the tensile response of the tuft, and can therefore be neglected to improve the computational efficiency of the model. To this purpose, homogenised instead of layer-by-layer orthotropic properties are also defined for the composite material surrounding the resin volume. The values of these properties, along with those of the resin, are listed in Table 1. Figure 6 shows the mesh developed in Abaqus 6.14 to simulate the response of the specimens described in Section 2.

3.2. Boundary conditions

For the model of Fig. 6, which is used to simulate the mechanical behaviour of a pre-delaminated single-tuft specimen under tensile loading, the x- and y- translations of all the nodes of the top and bottom surfaces of the composite have been set to zero. This accounts for the fact that, in the experiments, these surfaces are glued to the T-tabs through which the load is applied, as shown in Fig. 1. The bottom surface is further constrained in the z-direction, while displacement is applied to the top surface as a constant velocity. In the case where the finite element approach is applied to simulate the response of the unit cell of a tufted composite, symmetry boundary conditions must be applied to the edges parallel to the xz and yz planes.

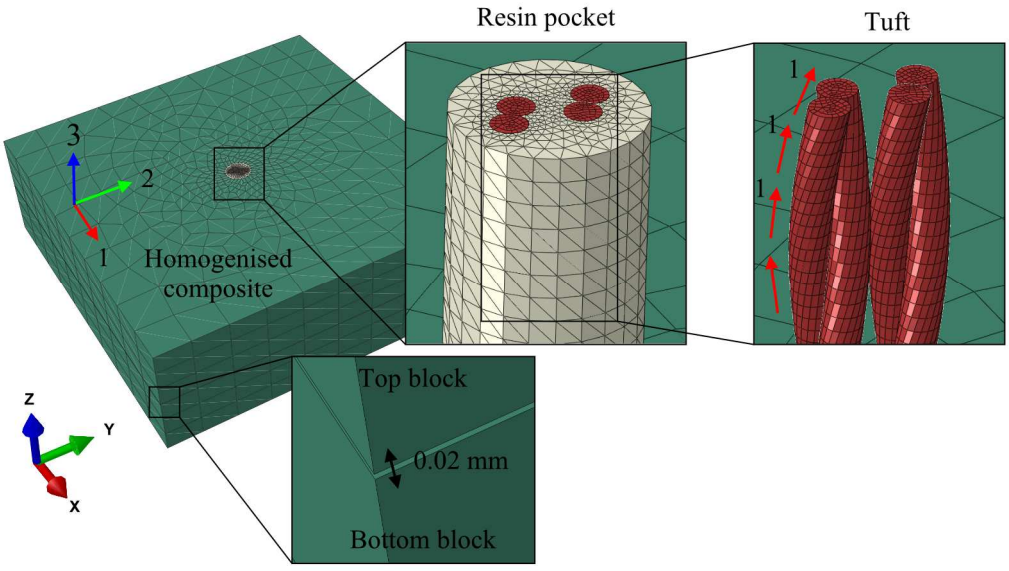

Figure 6. Full FE mesh of the modelled single-tuft coupon. A gap between the top and bottom half of the coupon has been left to account for the presence of the layer of release film (see Section 2). The model has been developed and analysed with Abaqus 6.14 (Explicit).

Excerpt from ISBN 978-3-00-053387-7

3.3. Simulation of debonding at the tuft-matrix interface

Progressive de-cohesion of the tuft from the surrounding laminate has been identified as one of the causes of the stiffness reduction observed in the mode I bridging response of tufts. In Abaqus 6.14, this dis-bond can be simulated by using a surface-based cohesive contact formulation or by introducing a layer of cohesive elements around each yarn. The mechanical behaviour of the zero-thickness tuft-matrix interface can then be described in terms of a 'traction versus separation' response [8, 9], dependent on the local mode-mixity. For the model in Fig. 6, a bilinear law has been selected to characterise the response of the tuft/matrix interface to peel and shear loading. Damage initiation has been defined using a quadratic nominal stress criterion, whereas a power law has been adopted to define failure. The expressions of the two criteria follow:

$$\left(\frac{\sigma_I}{\sigma_I^{\max}}\right)^2+\left(\frac{\sigma_{II}}{\sigma_{II}^{\max}}\right)^2=1 \qquad \text{Damage initiation criterion} \qquad (1)$$

$$\left(\frac{G_I}{G_I^{\,c}}\right)^{\alpha}+\left(\frac{G_{II}}{G_{II}^{\,c}}\right)^{\alpha}=1 \qquad \text{Failure criterion} \qquad (2)$$

where σ_I^{max} and σ_{II}^{max} are the peak values of the normal and transverse stresses at the interface, G_I^C and G_{II}^C are the fracture energies associated with mode I and mode II fractures respectively, and α is a coefficient commonly varying between 1 and 2 [10]. De-cohesion of a node (for cohesive contact) or element (for cohesive elements) in the model occurs when equation (2) is satisfied for that node/element. The parameters characterising the cohesive law of the interface are not known *a priori* and need to be calibrated by means of experimental data. Figure 7 shows the effect of variations of the mode II cohesive parameters on the response of the tuft. A reduction of σ_{II}^{max}, for fixed G_{II}^C (Fig. 7a), anticipates damage initiation and at the same time delays interfacial failure (i.e. debonding). A damaged interface translates in an overall more compliant tensile response of the tuft (i.e. it affects both the bonded and debonding stages of the response), as revealed by the results reported in Fig. 7a for a bonded tuft. Consequently, as a guideline to the calibration process, the interface shear strength should be chosen first to match the bonded response of the tuft. Then, the fracture energy should be varied to capture the average critical load marking the onset of debonding.

Excerpt from ISBN 978-3-00-053387-7

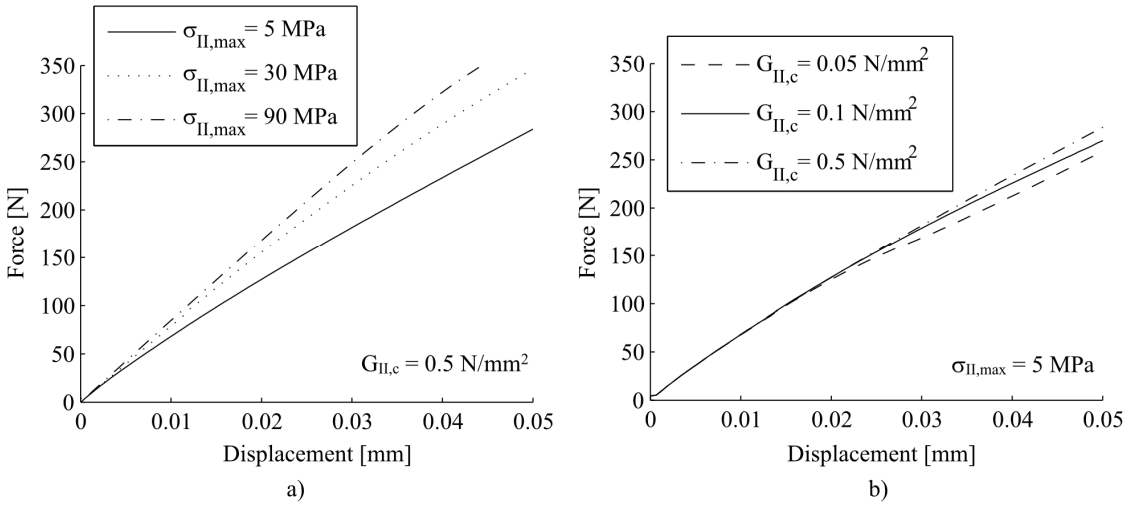

Figure 7. Parametric analysis: evaluation of the effect of interface cohesive parameters on the bridging law of the tuft. Curves in a) have been derived for $G_{II,c}$ = 0.5 N/mm^2, those in b) for $\sigma_{II,max}$ = 5 MPa. All the curves have been determined for a cohesive stiffness K = $\sigma_{II,max}/\delta_I$ = 10^5 N/mm^3. Cohesive contact has been used, in this case, to model the tuft/matrix interface.

A comparison between the curves in Fig. 7 and the experimental curve of Fig. 4 reveals that the amount of stiffness change due to progressive debonding is not sufficient to explain/capture the second stage of the tuft bridging response. This seems to suggest that other mechanisms come into play, which have not been accounted for as yet. The implementation of damage models into the material card of the helical yarns would enable to account for fibre-matrix splitting in the tuft before failure [7] and possibly help to fill this gap.

3.4. The role of thermal stresses

Residual stresses induced in the z-reinforced composite by the post-cure cool down process can promote failure in the tuft-matrix interface [8, 11]. Thermal residual stresses are caused by a mismatch in the coefficients of thermal expansion of the impregnated tuft and the resin material surrounding it (see Table 1), and they become more important the higher the cure temperature of the composite. A thermal analysis has been carried out for the system described in Section 2. A temperature variation of ΔT = -57 °C, corresponding to the difference between cure and room temperature, has been applied to the entire model. As is to be expected, residual stresses arise at the tuft-matrix interface and they are maximum close to the free edges of the helical yarns, i.e. at the delamination plane. They are tensile and shear stresses, which can anticipate, if not directly initiate, the damage that leads to debonding.

Excerpt from ISBN 978-3-00-053387-7

4. Conclusions

This paper has addressed the characterisation of mode I crack bridging via tufting and the development of a level-1 meso-scale finite element model for tufted composites. A method for the geometrical idealisation of tufts has been proposed which allows to account for fundamental features, such as the helical fibre architecture of the yarns, which induces a non-uniform stress distribution in the fibres and promotes mechanical interlocking between the tuft and surrounding composite. The process of progressive debonding, together with fibre-matrix splitting, have been identified as the main causes of stiffness reduction during mode I crack bridging by tufts. In the model, debonding is characterised through the cohesive parameters describing the mechanical response of the tuft-matrix interface. A parametric study has been carried out to understand the influence of variations of these cohesive parameters on the bridging law of the tuft. It has also been pointed out that thermal residual stresses could play an important role in facilitating debonding, especially in composites cured at relatively high temperatures. The introduction of a thermal step in the analysis of the model would enable to account for this effect in the mechanical response of the tuft.

Acknowledgments

The authors would like to acknowledge the Engineering and Physical Sciences Research Council (EPSRC) and Rolls-Royce plc for the support of this research through the Advanced Composites Centre for Innovation and Science (ACCIS) and the Composites University Technology Centre (UTC) at the University of Bristol, UK.

References

[1] G. Dell'Anno, J.W.G Treiber, I.K. Partridge, Manufacturing of composite parts reinforced through-thickness by tufting, *Robotics and Computer Integrated Manufacturing*, 37:262-272, 2016.
[2] G. Allegri, G. Mohamed, S.R. Hallett, Multi-scale modelling for predicting fracture behaviour of through-thickness reinforced laminates, *Numerical modelling of failure in advanced composite materials*, Elsevier Ltd., 2015.
[3] I.K. Partridge, S.R. Hallett, Use of microfasteners to produce damage tolerant composite structures, *Philosophical Transactions of the Royal Society A*, 2016 (accepted).
[4] F. Bianchi, X. Zhang, A cohesive zone model for predicting delamination suppression in z-pinned laminates, *Composites Science and Technology*, 71:1898-1907, 2011.
[5] A. Mouritz, B.N. Cox, A mechanistic interpretation of the comparative in-plane mechanical properties of 3D woven, stitched and pinned composites, *Composites Part A: Applied Science and Manufacturing*, 41:709-728, 2010.
[6] M. Sakai, R. Matsuyama, T. Miyajima, The pull-out and failure of a fibre bundle in a carbon fiber reinforced carbon matrix composite, *Carbon*, 38:2123-2131, 2000.
[7] S.V. Lomov et al., Meso-FE modelling of textile composites: Road map, data flow and algorithms, *Composites Science and Technology*, 67:1870-1891, 2007.
[8] B. Zhang, G. Allegri, M. Yasaee, S.R. Hallett, Micro-mechanical finite element analysis of Z-pins under mixed mode loading, *Composites: Part A*, 78:424-435, 2015.
[9] Y.Y. Jia, W. Yan, H.-Y. Liu, Numerical study on carbon fibre pullout using a cohesive zone model, *Proceedings of the 18th International Conference of Composite Materials ICCM18*, 2011.
[10] W.-G. Jiang, S.R. Hallett, B.G. Green, M.R. Wisnom, A concise interface constitutive law for analysis of delamination and splitting in composite materials and its application to scaled notched tensile specimens, *International Journal for Numerical Methods in Engineering*, 69:1982-1995, 2007.
[11] Y.Y. Jia, W. Yan, H.-Y. Liu, Carbon fibre pullout under the influence of residual thermal stresses in polymer matrix composites, Computational Materials Science, 62:79-86, 2012.

Excerpt from ISBN 978-3-00-053387-7